Proceedings of the ASME 2010 International Mechanical Engineering Congress & Exposition
IMECE2010
November 12-18, 2010, Vancouver, British Columbia, Canada

IMECE2010-39424

NUMERICAL EVALUATION OF SINGLE FIBER MOTION FOR SHORT FIBER COMPOSITES MATERIALS PROCESSING

Dongdong Zhang
Department of Mechanical & Aerospace Engineering
University of Missouri, Columbia, MO, USA
dz25c@mail.missouri.edu

Douglas E. Smith
Department of Mechanical & Aerospace Engineering
University of Missouri, Columbia, MO, USA
SmithDoug@missouri.edu

David A. Jack
Department of Mechanical Engineering
Baylor University, Waco, Texas, USA
David_Jack@baylor.edu

Stephen Montgomery-Smith
Department of Mathematics
University of Missouri, Columbia, MO, USA
stephen@missouri.edu

ABSTRACT

This paper presents a numerical approach for calculating the single fiber motion in a viscous flow. This approach addresses such issues as the role of axis ratio and fiber shape on the dynamics of a single fiber, which was not addressed in Jeffery's original work. We develop a Finite Element Method (FEM) for modeling the dynamics of a single rigid fiber suspended in a moving fluid. Low Reynolds number viscous flows are considered since these best represent the flow conditions for a polymer melt within a mold cavity. Our approach seeks the fiber angular velocities that zero the hydrodynamic torques acting on the fiber using the Newton-Raphson method. Fiber motion is then computed with a Runge-Kutta method to update the position, i.e. the angle of the fiber as a function of time. This method is quite general and allows for fiber shapes that include, but are not limited to, ellipsoidal fibers (such as that studied in Jeffery's original work), cylindrical fibers and beads-chain fibers. The relationships between equivalent axis ratios and geometrical axis ratios for cylindrical and beads-chain fibers are derived in this paper.

Keywords: Jeffery's obit, numerical methods, short-fiber composite, fiber orientation, equivalent axis ratio, cylindrical fiber, beads-chain fiber

1 INTRODUCTION

Mechanical properties of short-fiber-reinforced composite systems are largely dependent on the fiber orientation within the polymer matrix which is determined during the manufacturing process. The orientation state of the fibers is often computed based on the methods first proposed by Jeffery [1] which considered a single ellipsoidal fiber rotating in a Newtonian, incompressible homogeneous flow. Jeffery pointed out that fiber has a closed periodic tumbling motion within the fluid, often referred to as "Jeffery's orbit". Many researches [2]-[5] have observed this periodic phenomenon in experiments. But Taylor [2] found in the experiments that a fiber may deviate from Jeffery's orbit after a very long time, i.e. there exists a slow drift in Jeffery's orbit, which might result from the neglected terms in Jeffery's approximate equation.

To better understand the motion of a fiber, we developed a Finite Element Method (FEM) for modeling the dynamics of a single rigid fiber suspended in a moving fluid. Newton-Raphson and Runge-Kutta method are utilized to update the positions of fiber at select times. This methodology produces a reasonable agreement with Jeffery's solution provided the same assumptions apply. It could be extended to consider other effects, such as fluid inertia, so as to give more insights on explaining the small deviation in experiments.

Based on Jeffery's work, researchers extended to study fiber suspensions in broader areas [6][7]. Jia [8] considered the slip boundary condition on the fiber surface, while Jeffery applied the non-slip boundary condition. Junk [9] studied the effect of a bounded wall around the fiber, and pointed out that Jeffery's result represents the leading order equations of a singularly perturbed flow problem. Leal [7] analyzed the non-Newtonian effect of a fluid with the presence of fibers. In Jeffery's theory, fluid inertia and particle inertia are ignored, so Leal [7] studied the fiber motion under the consideration of weak fluid inertia and Altenbach [10] analyzed the influence of the rotary inertia. To study the non-dilute fiber suspension, Batchelor [11][12] proposed the constitutive model to take into account the contribution of fibers to the total stress tensor. Orientation averaging using Jeffery's approach has since yielded the orientation tensor methods [13], which are applied regularly today in industry. Many new closure approximations [14][15] have been developed to allow these orientation averaging approached to yield reasonably accurate results. With the understanding of rigid fiber migration within a viscous fluid, researchers moved on to the study of flexible fibers [16]-[18]. Yamamoto [16] regarded a fiber as a group of beads that are lined up and bonded to each neighbor as beads chain. Each pair of bonded spheres can stretch, bend and twist. Wang [17] used the rod-chain model to model the flexible fiber.

In this paper, we focus on the migration of fibers with axisymmetric shapes, such as cylindrical fibers and beads-chain fibers. One main factor that dictates Jeffery's orbit is the fiber's geometric axis ratio, obtained from the fiber's shape. The study of fibers with different shapes initiated from Bretherton [19], who proposed that Jeffery's theory is also valid for general axisymmetric bodies with fore-aft symmetry, and the equivalent axis ratio (r_e^*) is used, which differs from geometric axis ratio (r_e). For cylindrical fibers, the periodic orbit is observed in [3][5][20][21]. These authors found in experiments that the cylindrical fibers have different rotation periods from ellipsoidal fibers. Trevelyan [3] experimentally estimated the ratio of the equivalent axis ratio to the geometric axis ratio (r_e^*/r_e) to be approximately 0.7. Petrich [20] found that the ratio is 0.687 for $r_e = 50$ and 0.623 for $r_e = 72$. Cox [22] proposed the theoretical equation to calculate the equivalent axis ratio for slender cylindrical fibers, but the equation is not valid for short rod-like fibers, with an axis ratio smaller than 20. Additionally, we find that current simulation methods provide little attention to the motion of fibers with short geometric axis ratios.

Hence, in this paper, we study the equivalent axis ratios by using the Finite Element Method. We are able to numerically generate data that describes the relationships between the equivalent axis ratios and geometric axis ratios for cylindrical fibers over a wide range of axis ratios. The simulation results agree with the experimental data for short cylindrical fibers [5] and also conform to Cox's theory [22] for large-aspect-ratio cylindrical fibers. To verify our results, we numerically simulate the motion of a cylindrical fiber with geometric axis ratio, which is compared with that of an ellipsoidal fiber with the corresponding equivalent axis ratio. The two sets of data match very well. We also study the motion of beads-chain fibers, which is a good candidate to model flexible fibers [16]. The equivalent axis ratio for beads-chain fiber is derived in this paper. We validate our results by evaluating the motion of a beads-chain fiber, which is compared with that of an ellipsoidal fiber.

Above all, our main contributions in this paper are:

- **A methodology which combines the Finite Element Method, the Newton-Raphson method and the Runge-Kutta approach to study the dynamics of fiber motion within a fluid** In this methodology, the Finite Element Method is applied to solve the Navier-Stokes equation, so as to evaluate the hydrodynamic forces and torques on the fiber. The Newton-Raphson method is applied to search for angular velocities, which lead to zero torques exerted on the fiber. The Runge-Kutta method is utilized to update the fiber positions with respect to time. Our approach using ellipsoidal fibers yields the fiber angle as a function of time that exactly matches Jeffery's solution.
- **Equivalent axis ratios for cylindrical fibers and beads-chain fibers** The numerical data generated from our approach is valid for both short and slender fibers. Additional calculations are then performed to compare the fiber alignment rate of ellipsoidal fibers with that of cylindrical and beads-chain fibers, which confirms that the motions of axisymmetric fibers follows Jeffery's orbit, and the equivalent axis ratios derived from our numerical method are verified.

The paper is organized as follows. Section 2 presents the methodology, including the Finite Element Method, the Newton-Raphson method and the Runge-Kutta method. Section 3 derives the relationships between the equivalent axis ratios and geometric ratios for cylindrical fibers and beads-chain fibers. Implementation and illustrative examples are given in Section 4. Finally, conclusions and future work are presented in Section 5.

2 VALIDATION OF JEFFERY'S EQUATION

In this section, Jeffery's equation is revisited and validated by using our numerical schemes. This approach is not only applicable to ellipsoidal fibers, but also fibers of arbitrary shapes.

2.1 Jeffery's equation

Jeffery [1] proposed the method to solve Stokes equation with the moving boundary conditions in a local coordinates system

$x'y'z'$. This local coordinates system is rotating with respect to the global coordinates system xyz, shown in Fig.1.

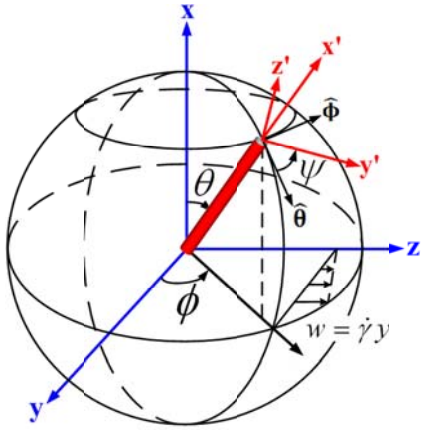

Fig.1 xyz is the global coordinate system translating with fiber but without rotation, and $x'y'z'$ is the local coordinate system translating and rotating with fiber. θ is the angle between x and x' axis, ϕ the angle between xy and xx' plane, and ψ the angle between y' and xx' plane.

By using Lamb's classic treatise [24] and assuming the free-torque particle, Jeffery solved the coupled Ordinary Differential Equations (ODEs), i.e. $\phi(t), \theta(t), \psi(t)$, for simple shear flow, where $\phi(t)$, $\theta(t)$, $\psi(t)$ are expressed as

$$\phi(t) = tan^{-1}\left(r_e tan\frac{\dot{\gamma}t}{r_e+\frac{1}{r_e}}\right) \quad (1)$$

$$\theta(t) = tan^{-1}\frac{Cr_e}{\sqrt{r_e^2 cos^2\phi + sin^2\phi}} \quad (2)$$

$$\psi(t) = \int_0^t (\frac{\dot{\gamma}}{2} - \dot{\phi})cos\theta dt \quad (3)$$

where r_e is the axis ratio of fiber, i.e. the ratio of semi-long axis and semi-short axis, $\dot{\gamma}$ the flow shear rate, C a constant of integration called the orbit constant, determined by the initial configuration of fiber orientation. C varies between 0 and $+\infty$. $C = 0$ corresponds to the fiber rolling along its symmetric axis, and $C = +\infty$ represents the periodic tumbling of fiber in the yz plane, shown in Fig.2(b). For axisymmetric fibers, we only take into account $\phi(t)$ and $\theta(t)$, because the rotation along fiber's symmetric axis has no effect on the fiber orientation. And by differentiating Eqn.(1), (2) and (3), the angular velocity $\dot{\phi}(t), \dot{\theta}(t), \dot{\psi}(t)$ can be obtained, with $\dot{\phi}(t)$ shown in Fig.2(a).

From Fig.2(b), we can see that the fiber motion follows Jeffery's orbit, with the period

$$T = \frac{2\pi}{\dot{\gamma}}\left(r_e + \frac{1}{r_e}\right) \quad (4)$$

which is only a function of the flow shear rate $\dot{\gamma}$ and the fiber's geometric axis ratio r_e. Hence, fiber shape has a great influence on the characteristics of fiber migration, which is studied in Section 3 in this paper.

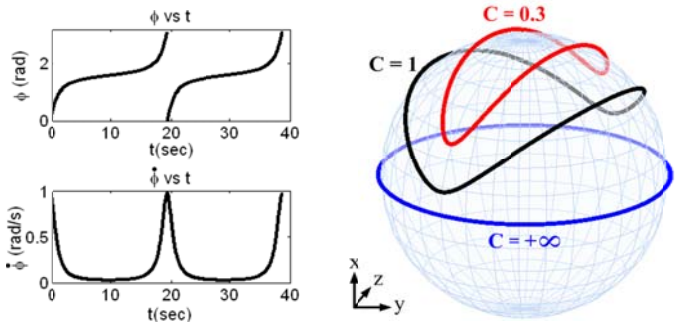

(a) **(b)**

Fig.2 (a) Distribution of $\phi(t)$ and $\dot{\phi}(t)$ in one period; (b) Jeffery's orbit with different orbit constant $C's$

2.2 Numerical validation

In recent years, computational methods [25][26] have been carried out to solve the fluid mechanics problems. In this section, we apply numerical schemes to solve the motion of a single fiber within a viscous fluid. In order to validate Jeffery's equation, we set the same conditions as those in Jeffery's paper. The basis is that the fiber is moving so as to produce no force and no torque from the fluid. An overview of the methodology is described below.

STEP 1: With a given ϕ_i, θ_i, ψ_i (i starts from 0), the finite element model for the fluid domain between fiber surface and far-away fluid boundary is defined. In this model, we need to know $\dot{\phi}_i, \dot{\theta}_i, \dot{\psi}_i$ to define the velocity boundary around fiber surface so as to calculate the force and torque exerted on fiber. Hence, the hydrodynamic torque (**M**) is a function of $\dot{\phi}, \dot{\theta}, \dot{\psi}$, denoted as $\mathbf{M}(\dot{\phi}, \dot{\theta}, \dot{\psi})$. Note that based on Jeffery's assumption, the desirable $\dot{\phi}_i, \dot{\theta}_i, \dot{\psi}_i$ give rise to zero torques on the fiber.

STEP 2: Use the Newton-Raphson method to find the expected $\dot{\phi}_i, \dot{\theta}_i, \dot{\psi}_i$, that generates zero torques along any spatial axis, i.e. solve $\mathbf{M}(\dot{\phi}, \dot{\theta}, \dot{\psi}) = \mathbf{0}$ for each time moment t_i.

Note that at different moments in time, the solution to $\mathbf{M}(\dot{\phi}, \dot{\theta}, \dot{\psi}) = \mathbf{0}$ is different, because the finite element model, defined by ϕ, θ, ψ, is changing with respect to time. Hence, we regarded $\dot{\phi}_i, \dot{\theta}_i, \dot{\psi}_i$ as a function of ϕ_i, θ_i and ψ_i, denoted here as $\dot{\mathbf{y}}_i = \boldsymbol{f}(t, \mathbf{y}_i)$, where $\mathbf{y}_i = [\phi_i, \theta_i, \psi_i]^T$.

STEP 3: Use a 4th order Runge-Kutta method to update ϕ_{i+1}, θ_{i+1}, ψ_{i+1} as follows:

$$\mathbf{y}_{i+1} = \mathbf{y}_i + \frac{\Delta t}{6}(\mathbf{k}_1 + \mathbf{k}_2 + \mathbf{k}_3 + \mathbf{k}_4) \quad (5)$$

where

$$\mathbf{k}_1 = \mathbf{f}(t_i, \boldsymbol{y_i})$$

$$\mathbf{k}_2 = \mathbf{f}\left(t_i + \frac{1}{2}\Delta t, \mathbf{y_i} + \frac{1}{2}\mathbf{k}_1\Delta t\right)$$

$$\mathbf{k}_3 = \mathbf{f}\left(t_i + \frac{1}{2}\Delta t, \mathbf{y_i} + \frac{1}{2}\mathbf{k}_2\Delta t\right)$$

$$\mathbf{k}_4 = \mathbf{f}(t_i + \Delta t, \mathbf{y_i} + \mathbf{k}_3\Delta t)$$

Therefore, with knowledge of only the starting angles ϕ_0, θ_0, ψ_0, the fiber's positions as a function of time can be steadily obtained, i.e. ϕ_i, θ_i, ψ_i and $\dot{\phi}_i, \dot{\theta}_i, \dot{\psi}_i$ for the fiber are updated as time increases. The details are illustrated as follows.

2.2.1 Finite element model The Finite Element Method is utilized to solve the velocity and pressure distribution within the fluid, so as to calculate the force and torque on the fiber. We use tetrahedral meshes to represent the fluid domain, with two velocity boundary conditions: far-away fluid velocity (BC1) and velocity on fiber surface (BC2), shown in Fig.3. For an axisymmetric fiber, such as an ellipsoid, only ϕ and θ, as defined in Fig.1, are needed to define the fiber's position.

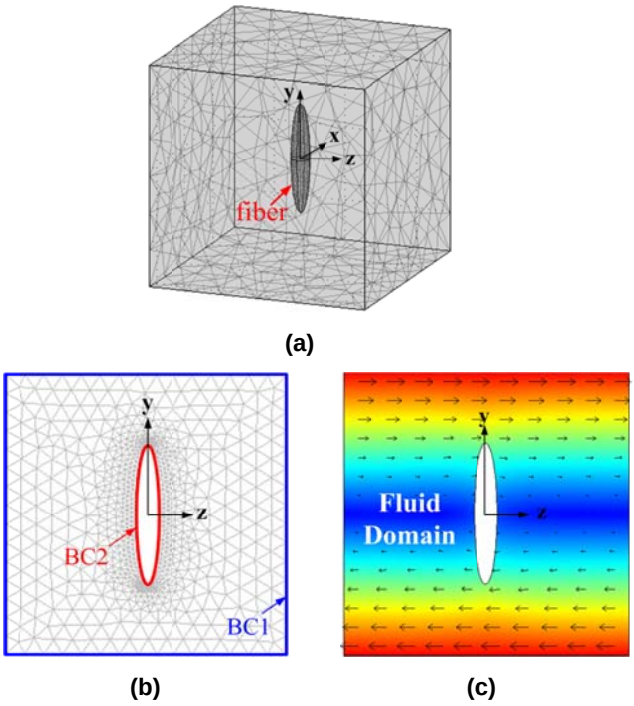

Fig.3 (a) 3D finite element model (Mesh model); (b) Mesh model in YZ plane with two velocity boundaries (BC1 and BC2); (c) Velocity distribution ($w' = \dot{\gamma} y$) in the yz plane.

In our model, all governing equations and boundary conditions are defined in the global coordinate system xyz, while Jeffery solved the problem in local coordinate system $x'y'z'$. Here, the governing equations in our model are

(1) Steady Navier-Stokes equation: $\rho \mathbf{U} \cdot \nabla \mathbf{U} = -\nabla p + \mu \nabla^2 \mathbf{U}$

(2) Continuity equation: $\nabla \cdot \mathbf{U} = 0$

where $\mathbf{U}$ represents the velocity distribution of fluid flow, p the pressure distribution, ρ the density of the fluid, μ the absolute viscosity of the fluid. And the velocity boundary conditions are

(1) For far-away fluid domain (BC1): $\mathbf{U} = \mathbf{L}\mathbf{x}$

(2) On the fiber surface (BC2): $\mathbf{U} = \mathbf{U_0} + B(\boldsymbol{\omega})\mathbf{x}$

where $\mathbf{U_0}$ is the translation velocity of the fiber centroid, which follows the movement of the fluid at that point. $\mathbf{L}$ is the velocity gradient, and for simple shear flow, $\mathbf{L} = \begin{pmatrix} 0 & 0 & 0 \\ 0 & 0 & 0 \\ 0 & \dot{\gamma} & 0 \end{pmatrix}$, in which $\dot{\gamma}$ is the flow shear rate. $\mathbf{x}$ is the displacement vector. $B(\boldsymbol{\omega})$ is the angular velocity matrix, defined as

$$B(\boldsymbol{\omega}) = \dot{\mathbf{R}}\mathbf{R}^{\mathrm{T}} = \begin{bmatrix} 0 & -\omega_z & \omega_y \\ \omega_z & 0 & \omega_x \\ -\omega_y & \omega_x & 0 \end{bmatrix} \tag{6}$$

where $\omega_x, \omega_y, \omega_z$ are the fiber angular velocities with respect to x, y, z axis respectively, defined as

$$\boldsymbol{\omega} = \begin{bmatrix} \omega_x \\ \omega_y \\ \omega_z \end{bmatrix} = \begin{bmatrix} \dot{\phi} + \dot{\psi}\cos\theta \\ -\dot{\theta}\sin\phi + \dot{\psi}\sin\theta\cos\phi \\ \dot{\theta}\cos\phi + \dot{\psi}\sin\theta\sin\phi \end{bmatrix} \tag{7}$$

And $\mathbf{R}$ is the direction cosine matrix, and $\dot{\mathbf{R}}$ the derivative of $\mathbf{R}$ with respect to time.

$$\mathbf{R} = \begin{bmatrix} l_1 & l_2 & l_3 \\ m_1 & m_2 & m_3 \\ n_1 & n_2 & n_3 \end{bmatrix} \tag{8}$$

where

$l_1 = \cos\theta$, $m_1 = \sin\theta\cos\phi$, $n_1 = \sin\theta\sin\phi$

$l_2 = -\sin\theta\cos\psi$, $m_2 = -\sin\phi\sin\psi + \cos\theta\cos\phi\cos\psi$

$n_2 = \cos\phi\sin\psi + \cos\theta\sin\phi\cos\psi$

$l_3 = \sin\theta\sin\psi$, $m_3 = -\sin\phi\cos\psi - \cos\theta\cos\phi\sin\psi$

$n_3 = \cos\phi\cos\psi - \cos\theta\sin\phi\sin\psi$

Therefore, in our finite element model, $\dot{\phi}_i$, $\dot{\theta}_i$, $\dot{\psi}_i$ determine the velocity boundary condition BC2, which affects the $\mathbf{U}$ and p within the fluid. After solving the finite element model, the net force $\mathbf{F}$ and torque $\mathbf{M}_o$ on the fiber can be obtained using the following equations

$$\boldsymbol{\sigma} = -p\boldsymbol{\delta}_{ij} + \mu[\nabla\mathbf{U} + (\nabla\mathbf{U})^{\mathrm{T}}] \tag{9}$$

$$\mathbf{F} = \int\{\boldsymbol{\sigma} \cdot \mathbf{n}\}\, dS \tag{10}$$

$$\mathbf{M}_o = \int\{\mathbf{x} \times (\boldsymbol{\sigma} \cdot \mathbf{n})\} dS \tag{11}$$

where μ is the absolute viscosity, $\boldsymbol{\delta}_{ij}$ Kronecker delta, and $\mathbf{n}$ the unit normal vector at fiber surface, $\mathbf{F} = F_x\mathbf{i} + F_y\mathbf{j} + F_z\mathbf{k}$, and $\mathbf{M}_o = M_x\mathbf{i} + M_y\mathbf{j} + M_z\mathbf{k}$.

Note that in order to verify Jeffery's orbit, we maintain the following conditions within our finite element model, which are analogous to Jeffery's assumptions:

a) Make sure the flow domain is much bigger than the fiber dimension, because Jeffery assumed the unbounded fluid domain in his paper. Hence, in our finite element model, we make $\varepsilon = \frac{fluid\ domain}{fiber\ size} \geq 40$.

b) The local Reynolds number $(Re = \frac{\rho U d}{\mu})$ is much smaller that 1, where ρ is the fluid density, μ absolute viscosity of fluid, U characteristic velocity and d characteristic length of fiber. Then the convection term $\rho\mathbf{U} \cdot \nabla\mathbf{U}$ in Navier-Stokes

equation can be neglected when solving the finite element model.

2.2.2 Search zero torque From section 2.2.1, we see that the hydrodynamic torque $\mathbf{M}_o$ is a function of $\dot{\phi}$, $\dot{\theta}$ and $\dot{\psi}$. Our purpose here is to find the exact $\dot{\phi}_{opt}, \dot{\theta}_{opt}, \dot{\psi}_{opt}$, which zero the torques M_x , M_y and M_z simultaneously, with the expression shown as follows.

$$\begin{cases} M_x(\dot{\phi},\dot{\theta},\dot{\psi}) = 0 \\ M_y(\dot{\phi},\dot{\theta},\dot{\psi}) = 0 \\ M_z(\dot{\phi},\dot{\theta},\dot{\psi}) = 0 \end{cases} \quad (12)$$

We use the Newton-Raphson method to solve $\dot{\phi}_{opt}, \dot{\theta}_{opt}, \dot{\psi}_{opt}$respectively by updating $\dot{\phi}_i$ $\dot{\theta}_i$ $\dot{\psi}_i$, shown as

$$[\dot{\phi}_{i+1} \ \dot{\theta}_{i+1} \ \dot{\psi}_{i+1}]^{\mathrm{T}} = [\dot{\phi}_i \ \dot{\theta}_i \ \dot{\psi}_i]^{\mathrm{T}} - [\boldsymbol{J_i}]^{-1}[\boldsymbol{F_i}] \quad (13)$$

where $[\boldsymbol{F_i}]$ is the torque vector evaluated at $[\dot{\phi}_i \ \dot{\theta}_i \ \dot{\psi}_i]^{\mathrm{T}}$, shown as

$$[\boldsymbol{F_i}] = \begin{bmatrix} M_x(\dot{\phi}_i,\dot{\theta}_i,\dot{\psi}_i) \\ M_y(\dot{\phi}_i,\dot{\theta}_i,\dot{\psi}_i) \\ M_z(\dot{\phi}_i,\dot{\theta}_i,\dot{\psi}_i) \end{bmatrix} \quad (14)$$

And $[\boldsymbol{J_i}]$ is the Jacobian matrix evaluated at $[\dot{\phi}_i \ \dot{\theta}_i \ \dot{\psi}_i]^{\mathrm{T}}$, shown as

$$[\boldsymbol{J_i}] = \begin{bmatrix} \frac{dM_x}{d\dot{\phi}}(\dot{\phi}_i,\dot{\theta}_i,\dot{\psi}_i) & \frac{dM_x}{d\dot{\theta}}(\dot{\phi}_i,\dot{\theta}_i,\dot{\psi}_i) & \frac{dM_x}{d\dot{\psi}}(\dot{\phi}_i,\dot{\theta}_i,\dot{\psi}_i) \\ \frac{dM_y}{d\dot{\phi}}(\dot{\phi}_i,\dot{\theta}_i,\dot{\psi}_i) & \frac{dM_y}{d\dot{\theta}}(\dot{\phi}_i,\dot{\theta}_i,\dot{\psi}_i) & \frac{dM_y}{d\dot{\psi}}(\dot{\phi}_i,\dot{\theta}_i,\dot{\psi}_i) \\ \frac{dM_z}{d\dot{\phi}}(\dot{\phi}_i,\dot{\theta}_i,\dot{\psi}_i) & \frac{dM_z}{d\dot{\theta}}(\dot{\phi}_i,\dot{\theta}_i,\dot{\psi}_i) & \frac{dM_z}{d\dot{\psi}}(\dot{\phi}_i,\dot{\theta}_i,\dot{\psi}_i) \end{bmatrix} \quad (15)$$

where the elements are evaluated using forward finite difference method. For example,

$$\frac{dM_x}{d\dot{\phi}} = \frac{M_x(\dot{\phi}_i + \Delta\dot{\phi}, \dot{\theta}_i, \dot{\psi}_i)}{\dot{\phi}_i + \Delta\dot{\phi}} \quad (16)$$

The same method can be used to evaluate other eight elements in the Jacobian matrix.

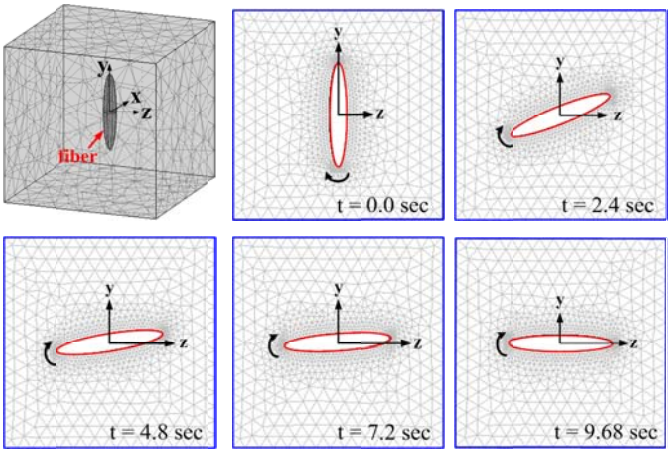

Fig.4 Fiber migration simulation by using numerical methods in simple shear flow ($w' = \dot{\gamma}y$). Upper left: 3D finite element model; Others: fiber migration at select moments in time shown in the yz plane

Therefore, in any moment t_i, we search for the right $\dot{\phi}_i$, $\dot{\theta}_i$, $\dot{\psi}_i$, which zero the torques exerted on the fiber. And the velocities are substituted into Eqn.(5) to update the fiber position for the next time step t_{i+1}. The migration of the fiber is displayed in Fig.4.

3 EQUIVALENT AXIS RATIOS FOR SYMMETRIC FIBERS WITH FORE-AFT SYMMETRY

Jeffery's equation is derived based on an ellipsoidal fiber. In this section, we analyze the orientations of fibers with other axisymmetric shapes, such as cylindrical and beads-chain fibers.

In Bretherton [19] and Cox [22]'s work, the symmetric fibers are demonstrated to have a similar periodic tumbling motion to that observed for ellipsoidal fibers, but the equivalent axis ratio r_e^* is utilized to quantify the fiber motion instead of the geometric axis ratio r_e. In [19] and [22], only slender fibers with large r_e are considered, and Cox's theoretical derivation for r_e^* does not apply to short fibers. In this paper, we use numerical methods to calculate the equivalent axis ratios of axisymmetric fibers with fore-aft geometry. And we use the methodology, proposed in Section 2, to simulate the migration of cylindrical fibers within a fluid, and compare with that of an ellipsoidal fiber.

For simple shear flow ($w' = \dot{\gamma}y$), when we consider the fiber motion with an orbit constant $C = +\infty$, we have $\theta = \frac{\pi}{2}, \psi = 0$ and $\dot{\theta} = \dot{\psi} = 0$ in Eqn.(7). So we have

$$\boldsymbol{\omega} = \begin{bmatrix} \omega_x \\ \omega_y \\ \omega_z \end{bmatrix} = \begin{bmatrix} \dot{\phi} \\ 0 \\ 0 \end{bmatrix}$$

where $\dot{\phi}$ is obtained by differentiating Eqn.(1) with respect to time. So

$$\omega_x = \dot{\phi} = \frac{\dot{\gamma}}{r_e^2+1}[r_e^2 + (1 - r_e^2)cos\phi] \quad (17)$$

And in [22], Cox considered the angular velocity ω_x and torque M_x when the fiber's axis is in a vertical direction ($\phi = 0$) and a horizontal direction ($\phi = \pi/2$) direction, shown in Fig.5.

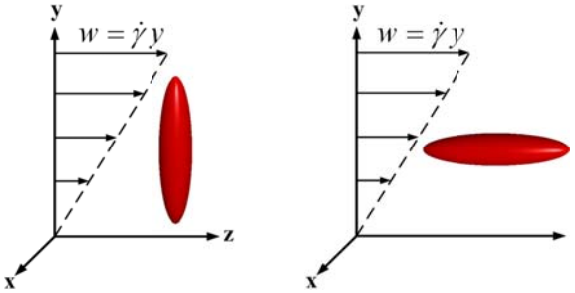

(a) Vertical direction **(b) horizontal direction**

Fig.5 (a) fiber fixed in the vertical direction ($\phi = 0$); (b) fiber fixed in the horizontal direction ($\phi = \pi/2$)

In the horizontal direction ($\phi = 0$), $[\omega_x]_H = \frac{\dot{\gamma}}{r_e^2+1}$, and in the vertical direction ($\phi = \pi/2$), $[\omega_x]_V = \frac{\dot{\gamma}}{r_e^2+1} r_e^2$. If we suppose that the fiber is fixed in both directions, a fiber will have torques exerted by the surrounding fluid, with the torques in two directions denoted as $[M_x]_H$ and $[M_x]_V$.

Cox [22] proposed that M_x should be proportional to fiber's angular velocity ω_x and the equivalent axis ratio is defined as

$$r_e^* = \sqrt{\frac{[\omega_x]_H}{[\omega_x]_V}} = \sqrt{\frac{[M_x]_H}{[M_x]_V}} \qquad (18)$$

The key point is to calculate fiber angular velocities or torques when the fiber is at rest. In this paper, the numerical method is used to calculate the torque in both orientation directions. Then the equivalent axis ratio is derived from Eqn. (18).

In this paper we focus on cylindrical and bead-model fibers, with the results showed in Section 4. The torques in the vertical and horizontal directions can be calculated by obtaining the velocity and pressure distribution in Finite Element Method. In the model, the velocity boundary condition at fiber surface is $\mathbf{U} = \mathbf{0}$, i.e. fiber is fixed within the fluid without translation and rotation. We derived the relationships between the equivalent axis ratios and the geometric axis ratios. The results for cylindrical fibers are consistent with the experimental results for short rod-like fibers, and also in accordance with Cox's theoretical derivation for slender fibers. We also use the methodology, proposed in Section 2, to derive the motion of cylindrical and beads-model fibers within a viscous fluid, and compare the results with that of ellipsoidal fibers whose geometric axis ratio equals to the equivalent axis ratios of cylindrical and beads-chain fibers. Note that the geometric axis ratio is defined as the ratio of the height and the radius for a cylindrical fiber, and number of beads for a beads-chain fiber. The simulation results are summarized in Section 4.

4 IMPLEMENTATION AND EXAMPLES

We implemented our numerical schemes by using COMSOL [27] and Matlab [28]. COMSOL is used to implement the computational fluid dynamics, and Matlab to search $\dot{\phi}, \dot{\theta}, \dot{\psi}$ and update angles as a function of time. In this section, several examples are presented to illustrate and validate the proposed approach.

4.1 Validation of Jeffery's orbit

In this section, we numerically simulate the motion of an ellipsoidal fiber in simple shear flow and Table 1 shows the parameters for our finite element model. In this example, we only update ϕ and θ, because ψ has no effect on the fiber orientation.

Table 1. Ellipsoidal fiber motion in simple shear flow

Finite element model	Ellipsoidal fiber	Semi-long axis: $1.5m$ Semi-short axis: 0.25m Geometric axis ratio: $r_e = r_e^* = 6$
	Boundary of Fluid domain	Length of cubic domain: 120m
Fluid Para-meters	Simple shear flow	$w = \dot{\gamma} y$ where $\dot{\gamma} = 1$
	Fluid density	$\rho = 1(kg/m^3)$
	Fluid absolute viscosity	$\mu = 100(kg/m \cdot s)$

The results from our numerical method are overlapped with Jeffery's solution in Fig.6.

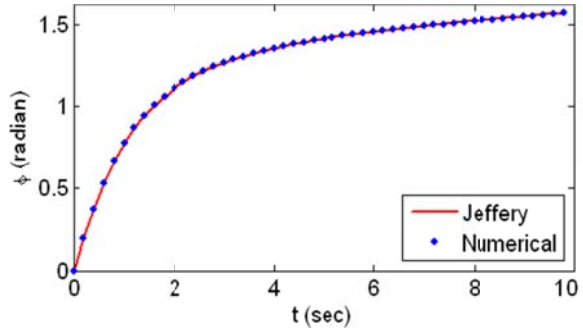

(a)

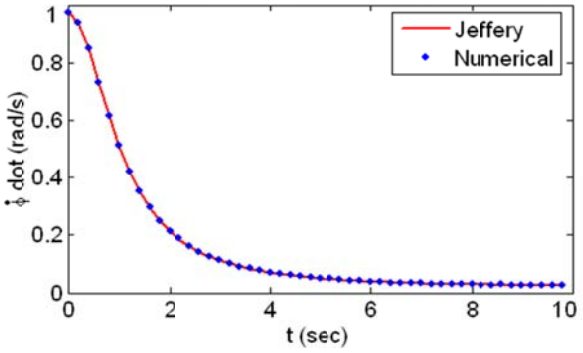

(b)

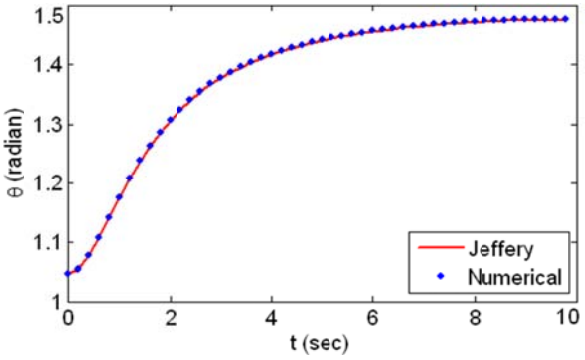

(c)

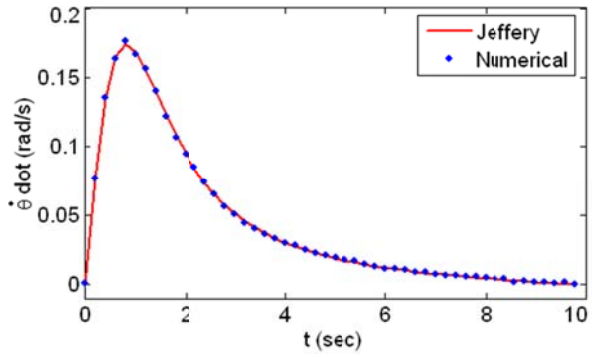

(d)

Fig.6 Numerical results of the single fiber motion in 1/4 period: (a) change of ϕ; (b) change of $\dot{\phi}$; (c) change of θ; (d) change of $\dot{\theta}$.

The comparison of two sets of data, i.e. Jeffery's data and our numerical data, are analyzed in Table 2. In this example, we choose $\Delta t = 0.2$ seconds for the Runge-Kutta method.

Table 2. Comparison between Jeffery's solution and our numerical data

Data Sets	Mean of absolute errors	Std. of absolute errors
ϕ (radians)	0.0018269	0.0013376
$\dot{\phi}$ (rad/s)	0.00019625	0.001266
θ (radians)	-0.0009395	0.00037811
$\dot{\theta}$ (rad/s)	-8.5666e-005	0.00085256

4.2 Equivalent axis ratios

In this section, we numerically determine the equivalent axis ratios for ellipsoidal, cylindrical and beads-chain fibers over a large range of axis ratios.

4.2.1 Ellipsoidal fibers Our numerical data of the equivalent axis ratios for ellipsoidal fibers are tabulated in Table 3.

Table 3. Equivalent axis ratios for ellipsoidal fiber

Geometric Axis ratio	Equivalent axis Ratio	Relative True Error
1	1.0081	0.008106
5	5.0081	0.0016246
10	9.9056	0.0094404
15	14.851	0.009953
20	20.146	0.0073192
30	29.999	3.89E-5
40	39.603	0.0099224
50	49.903	0.0019434
60	59.157	0.014058

From Table 3, we can see that, for ellipsoidal fibers, the equivalent axis ratio is the same as geometric axis ratio. Next, we derive the numerical data of equivalent axis ratios for cylindrical and beads-chain fibers.

4.2.2 Cylindrical fibers For cylindrical fibers, the geometric axis ratio is defined as the ratio of the height and the diameter. The equivalent axis ratio for a cylinder is derived by evaluating the torques in the vertical and horizontal directions, shown in Fig.7. The relations between equivalent axis ratio r_e^* and geometric axis ratio r_e are shown in Fig.8, in which We overlap our numerical data with that from Cox's theoretical equation[22] for slender fibers and Anczurowski's experiment [5].

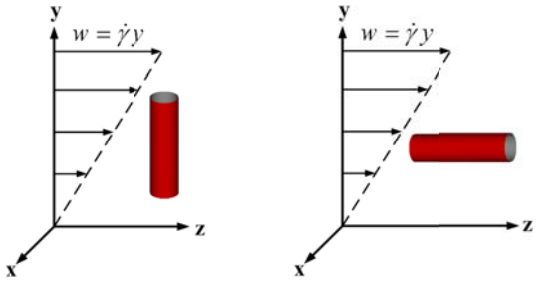

(a) **(b)**

Fig.7 (a) fiber fixed in the vertical direction; (b) fiber fixed in the horizontal direction

In Cox's theory, the equivalent axis ratio is derived from

$$r_e^* = r_e 1.24\sqrt{\ln(r_e)}$$

Anczurowski fitted the experimental data with a straight line, with the equation shown as follows. He pointed out that $r_e^* = r_e$ when $r_e = 1.68$ for cylindrical fiber.

$$r_e^* = 0.829 r_e - 0.287$$

In Fig.8, we compare our numerical data with Cox's equation and Anczurowski's fitted line. And the data is tabulated in Table 4.

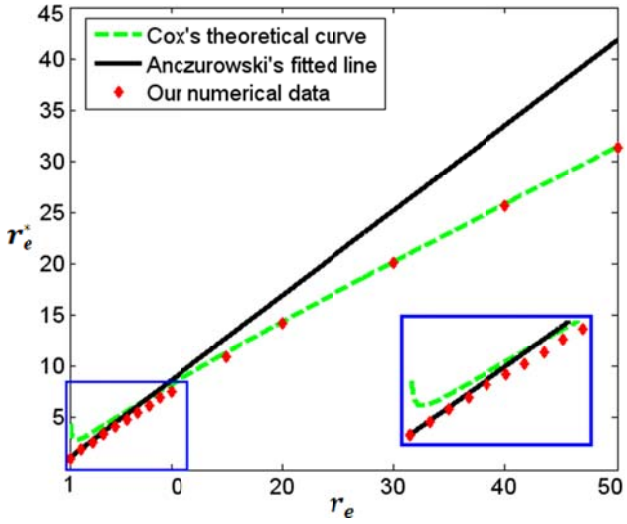

Fig.8 Comparison of our numerical data (red diamonds) with Cox's theoretical curve (dashed green curve) for slender fibers and Anczurowski's experimental results (solid black line)

From Fig.8, we can see that for short fibers, our numerical data is quite close to Anczurowski's fitted straight line, whereas for larger aspect ratios, our data corresponds quite well with that of Cox's theory for slender fibers when $r_e > 20$. The transition between the two models occurs as the axis ratio increases from a short fiber to a long fiber, and is well captured as can be seen from our numerical data, shown in Table 4.

Table 4. Equivalent axis ratio for cylindrical fibers

Geometric axis ratio	Equivalent axis ratio		
	Our data	Cox	Anczurowski
1	1.1168	Inf	1.2129
2	1.9415	2.9788	1.8969
3	2.7094	3.5491	2.5337
4	3.4292	4.2126	3.1305
5	4.1523	4.8871	3.7302
6	4.8476	5.5582	4.3068
7	5.4699	6.2224	4.8229
8	6.1787	6.8792	5.4106
9	6.9182	7.5288	6.0239
10	7.5891	8.1717	6.5802
15	10.899	11.303	9.325
20	14.193	14.328	12.057
30	20.122	20.171	16.974
40	25.676	25.825	21.58
50	31.355	31.347	26.289

In Section 4.3, we use the numerical schemes proposed in Section 2 to simulate the evolution of a single cylindrical fiber with $r_e = 6$, and conclude that our numerical data generate more accurate results than those of Cox [22] and Anczurowski [5].

4.2.3 Beads-chain fiber For a beads-chain fiber, the geometric axis ratio is defined as the number of beads connected together. The geometric aspect ratio is 4. We generate our numerical data for the beads-chain fiber by calculating the torques when the fiber is at rest in the two directions, shown in Fig.9. The equivalent axis ratios are shown in Fig.10, with the numerical data tabulated in Table 5.

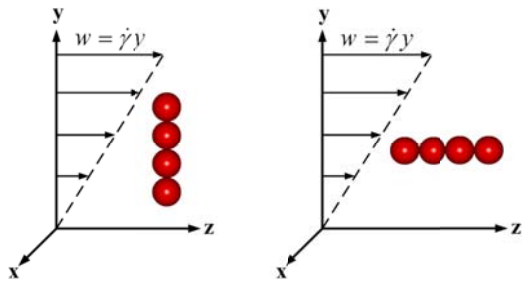

(a) (b)

Fig.9 (a) fiber fixed in the vertical direction ($\phi = 0$); (b) fiber fixed in the horizontal direction ($\phi = \pi/2$).

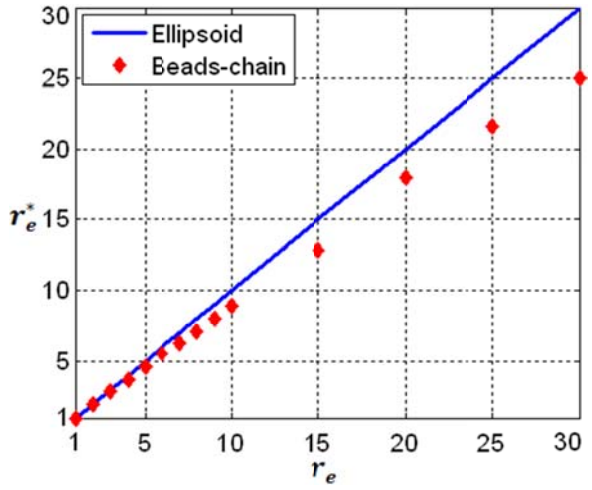

Fig.10 Equivalent axis ratios for beads-chain fibers (red diamonds) compared with ellipsoidal fibers (blue solid line)

From Fig.10, we see that the equivalent axis ratios are close to those of ellipsoidal fibers ($r_e^* = r_e$) with small axis ratios, but for slender fibers, the equivalent axis ratios deviate largely from those of ellipsoidal fibers.

Table 5. Equivalent axis ratio for beads-chain fibers

Geometric axis ratio	Equivalent axis ratio		Geometric axis ratio	Equivalent axis ratio
1	1		8	7.1196
2	1.9897		9	8.0313
3	2.8868		10	8.8975
4	3.7314		15	12.864
5	4.6173		20	17.978
6	5.5656		25	21.66
7	6.2593		30	25.052

4.3 Validation of equivalent aspect ratios

In Section 4.2, we derived the equivalent aspect ratios for cylindrical and beads-chain fibers. In this section, we use the methodology, proposed in Section 2 to validate our numerical data for equivalent aspect ratios.

4.3.1 Validation for cylindrical fibers From Table 4, the cylindrical fiber with $r_e = 6$ has the equivalent axis ratio $r_e^* = 4.8476$ in our results, whereas $r_e^* = 5.5582$ in Cox's theory and $r_e^* = 4.3068$ from Anczurowski's fitted straight line.

The evolution of ϕ and θ are is shown in Fig.11, in which the motion of an cylindrical fiber is obtained by the methodology proposed in Section 2, while the motion of an ellipsoidal fiber is evaluated from Jeffery's analytical solution.

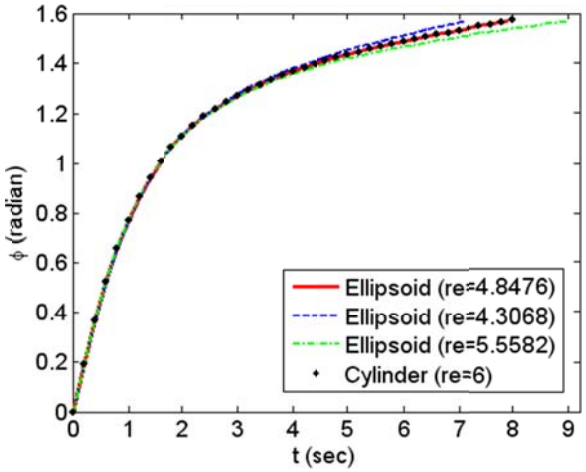

(a)

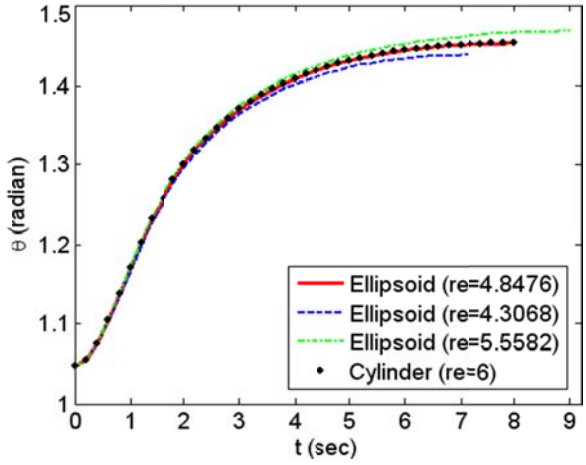

(b)

Fig.11 Evolution of a cylindrical fiber with geometric axis ratio $r_e = 6$ and an ellipsoidal fiber motion with $r_e = 4.8476$, 4.3068 and 5.5582: (a) change of ϕ; (b) change of θ

In Fig.11, we can see that the motion of a cylindrical fiber with $r_e = 6$ matches that of an ellipsoidal fiber with $r_e = 4.8476$, which is obtained from our result. We draw the conclusion that our numerical data for the equivalent axis ratios produces better results.

4.3.2 Validation for beads-chain fiber Similarly, we evaluate the motion of a beads-chain fiber with $r_e = 6$, and compare it with that of an ellipsoidal fiber with $r_e = 5.5656$, obtained from our numerical data. The results are shown in Fig.12. The motion of a beads-chain fiber is evaluated by our numerical schemes, and the motion of an ellipsoidal fiber is obtained from Jeffery's analytical solution.

From Fig.12, we can see the beads-chain with the geometric axis ratio $r_e = 6$ has the same rotational movement as that of the ellipsoidal fiber with $r_e = 5.5656$, which verify that our numerical data for equivalent axis ratios of beads-chain fibers is accurate.

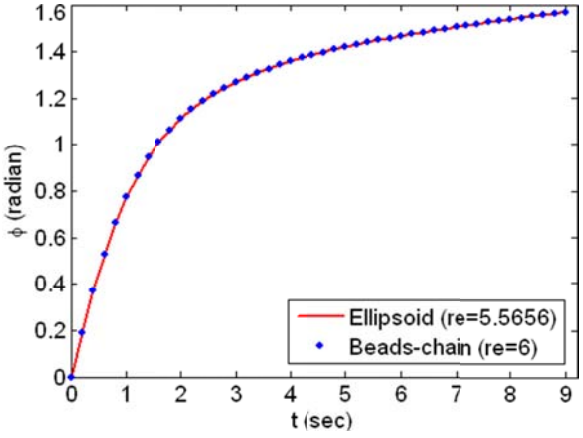

(a)

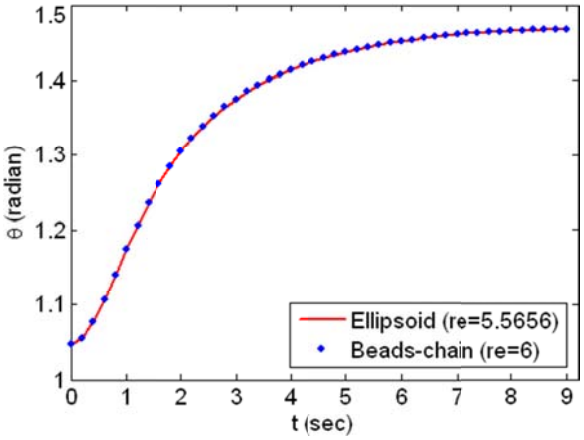

(b)

Fig.12 Evolution of a beads-chain fiber with geometric axis ratio $r_e = 6$ and an ellipsoidal fiber with $r_e = 5.5656$: (a) change of ϕ; (b) change of θ.

5 CONCLUSIONS AND FUTURE WORK

This paper presents a numerical approach to validate Jeffery's equation. The Finite Element Method is used to solve the Navier-Stokes equation, so as to calculate the hydrodynamic forces and torques on a fiber. Then the Newton-Raphson method is performed to numerically obtain the angular velocities, which zero the torques on the fiber. Lastly, a Runge-Kutta approach is utilized to trace the fiber orientations as a function of time. With the presented numerical methods, we are able to study the motion of cylindrical and beads-chain fibers, and present the numerical data for equivalent axis ratios of both fiber types.

Further work will include the study of fiber motion in a non-homogeneous flow, such as Poiseuille flow. A study of fiber-fiber interaction in a non-dilute flow will also be part of our future work. Meanwhile, we will derive the fiber motion with the consideration of other physical characteristics of fluid flow, such as weak fluid inertia and non-Newtonian effects. Finally, we will extend our methodology to study flexible fibers by modeling the fiber surface as a deformable boundary in the finite element model.

ACKNOWLEDGEMENTS

The financial support from the National Science Foundation through CMMI-MPM (NSF grant #0727399) is gratefully acknowledged.

REFERENCES

[1] Jeffery, G. B., 1922, "The motion of ellipsoidal particles immersed in a viscous fluid", Proceedings of the Royal Society of London. Series A, Containing Papers of a Mathematical and Physical Character, Vol. 102, Iss. 715, pp. 161-179.

[2] Taylor, G. I., 1923, "The Motion of Ellipsoidal Particles in a Viscous Fluid", Proceedings of the Royal Society of London. Series A, Containing Papers of a Mathematical and Physical Character, Vol. 103, No. 720, pp. 58-61.

[3] Trevelyan, B. J. and Mason, S.G., 1951, "Particle Motions in Sheared Suspensions. I. Rotations," Journal of Colloid Science, Vol. 6, pp. 354-367.

[4] Mason, S. G. and Manley, R. S. J., 1956, "Particle motions in sheared suspensions: Orientation and interactions of rigid rods", Proc. Roy. Soc. London, Vol. 238, No. 1212, pp.117-131.

[5] Anczurowski, E. and Mason, S. G., 1968, “Particle motions in sheared suspensions. XXIV. Rotation of rigid spheroids and cylinders”, Transactions of the Society of Rheology, Vol. 12, Iss. 2, pp. 209-215.

[6] Christopher J. S. Petrie, 1999, "The rheology of fiber suspensions", Journal of Non-Newtonian Fluid Mechanics, Vol. 87, Iss. 2-3, pp. 369-402.

[7] Leal, L. G., 1980, “Particle motions in a viscous fluid”, Annual Review of Fluid Mechanics, Vol. 12, Iss. 1, pp. 435-476.

[8] Jia, L., 2006, "Flow-induced alignment migration of particles in suspensions", PhD Dissertation, Department of Mechanical Engineering, Michigan State University.

[9] Junk, M. and Illner, R., 2007, "A New Derivation of Jeffery's Equation", Journal of Mathematical Fluid Mechanics, Vol. 9, No. 4, pp. 445-288.

[10] Altenbach, H., Brigadnov, I. and Naumenko, K., 2009, “Rotation of a slender particle in a shear flow: influence of the rotary inertia and stability analysis”, Journal of Applied Mathematics and Mechanics, Vol. 89, Iss. 10, pp. 789 - 870.

[11] Batchelor, G. K., 1970, "The stress system in a suspension of force-free particles", Journal of Fluid Mechanics, Vol.41, pp. 545-570.

[12] Batchelor, G. K, 1970, "Slender body theory for particles of arbitrary cross-section in Stoke flow", Journal of Fluid Mechanics, Vol. 44, pp. 419-440.

[13] Advani, S. G. and Tucker, C. L., 1987, "The use of Tensors to describe and predict fiber orientation in short fiber composites", Journal of Rheology, Vol. 31, Iss.8, pp. 751-784.

[14] Cintra, J. S. and Tucker III, C. L., 1995, "Orthotropic closure approximations for flow-induced fiber orientation", Journal of Rheology, Vol. 39, Iss. 6, pp. 1095-1122.

[15] Jack, D. A. and Smith, D. E., 2005, “An invariant based fitted closure of the sixth-order orientation tensor for short-fiber suspensions”, Journal of Rheology, Vol. 49, Iss. 5, pp.1091-1115.

[16] Yamamoto, S. and Matsuoka, T., 1993, “A method for dynamic simulation of rigid and flexible fibers in a flow field”, Journal of Chemical Physics, Vol. 98, Iss. 1, pp.644-650.

[17] Wang, G., Yu, W., and Zhou, C., 2006, “Optimization of the rod chain model to simulate the motions of a long flexible fiber in simple shear flows”, European Journal of Mechanics - B/Fluids, Vol. 25, Iss. 3, pp. 337-347.

[18] Switzer III, L. H., 2002, “Simulating systems of flexible fibers”, PhD Dissertation, Chemical Engineering, University of Wisconsin-Madison.

[19] Bretherton, F. P., 1962, "The motion of rigid particles in a shear flow at low reynolds number", Journal of Fluid Mechanics, Vol.14, Iss. 2, pp. 284-304.

[20] Petrich, M. P., Koch, D. L.& Cohen C., 2000, "An experimental determination of the stress-microstructure relationship in semi-concentrated fiber suspension", Journal of Non-Newtonian Fluid Mechanics, Vol. 95, Iss. 2-3, pp.101-133.

[21] Harris, J. B. and Pittman, J. F. T., 1975, “Equivalent ellipsoidal axis ratios of slender rod-like particles”, Journal of Colloid and Interface Science, Vol. 50, No. 2, PP. 280-282.

[22] Cox, R. G., 1971, "The motion of long slender bodies in a viscous fluid. Part2. shear flow", Journel of Fluid Mechanics, Vol. 45, part 4, pp.625-657.

[23] Kittipoomwong, P., See, H. and Mai-Duy, N., “Dynamic simulation of non-spherical particulate suspensions”, Rheologica Acta, Vol. 49, No. 6, pp. 597-606.

[24] Lamb, H., 1916, “Hydrodynamics”, Cambridge university press.

[25] Durbin, P. A. and Medic, G., 2007, “Fluid Dynamics with a computational perspective”, Cambridge University Press.

[26] Löhner, R., 2007, “Applied CFD techniques, an introduction based on Finite Element Method”, John Wiley & Sons, Ltd., second edition.

[27] http://www.comsol.com/

[28] http://www.mathworks.com/